Numerical Analysis on the Turbulent Flow of Compressor Cascades at High Incidence Angle

Soo-in Jeong[1], Gi-ho Jeong[1], Kui-soon Kim[2]
1. The graduate school of Aerospace Engineering department of Pusan National University
2. Department of Aerospace Engineering, Pusan National University
30 Jangejon-dong, Geumjeong-gu, Busan, 609-735, KOREA
sooin@pusan.ac.kr

Keywords: DCA cascade, incidence angle, SIMPLE/PWIM, turbulence flow

Abstract

A numerical analysis based on two-dimensional and three-dimensional incompressible Navier-Stokes equations has been carried out for double-circular-arc (DCA) compressor cascades. Two types of double-circular-arc cascades were used in this analysis. The appropriate turbulence model for compressor analysis was selected among the conventional turbulence models such as Baldwin-Lomax, k-ε and k-ω models. The results of current study were compared with available experimental data at various incidence angles. The 2-D and 3-D computational codes based on SIMPLE/PWIM algorithm for collocated grid and hybrid scheme for the convective terms were the main features of numerical tools. As commonly known, turbulence modeling is very important for the prediction of cascade flows, which are extremely complex with separation and reattachment by adverse pressure gradient. For selection of turbulence model, 2-D analysis was performed. And then, k-ε turbulence model with wall function chosen as the reasonable turbulence model for 3-D calculation was used to increase the efficiency of computation times. A reasonable result of 3-D flow pattern passing through the double-circular-arc cascade was obtained.

Introduction

The evaluation of gas turbine engine performance is strongly dependent on those of primary components such as compressor and turbine. Especially compressor performance is highly dependent on the operating conditions. Flow through the compressor is characterized as three dimensional, unsteady and turbulent flow that is always not easy to analyze. Furthermore, high incidence angle makes the flow drastically separated from the surface of compressor cascades.

In addition, some complex flow patterns caused by miscellaneous non-uniform factors occur simultaneously such as stall, surge, tip-clearance and secondary flows in rotor and stator. So, it is apparent that the flow through compressor cascade is obviously one of the most complicated flows to study. A number of studies on compressor cascade flow have been performed with experiments and various numerical methods. These studies have mostly considered compressors being operated in design conditions of low incidence.

Due to the lack of the performance data on off-design operations, the conventional investigations of the gas turbine engine performance used to ignore the off-design regions of operation, for instances, starting and warming-up of engine. It is a matter of course to get the sufficient performance data on operations in high incidence prior to the evaluation of gas turbine engine performance as a whole.

In this study, using various turbulence models like Baldwin-Lomax, k-ε and k-ω models, the study of turbulence models which could predict the flow characteristics of compressor cascades with more efficiency and accuracy has been made. And the numerical analyses of compressor cascade have been performed with the numerical tool developed here to consider a three dimensional, steady and incompressible turbulent flow through cascade at high incidence angle. The Mach number of compressor inlet condition in present study was so small (about 0.1) that the compressible effect could be neglected.

Two types of double-circular-arc cascade (DCA1, DCA2) which could be described as simple functions were selected as compressor cascade.

Numerical Method

Governing Equations

The flow through the compressor cascade could be governed by the steady, incompressible and three-dimensional Navier-Stokes equation.

$$\frac{\partial}{\partial x_j}\left(\rho u_j \Phi - \Gamma_\Phi \frac{\partial \Phi}{\partial x_i}\right) = S_\Phi \qquad (1)$$

- mass conservation

$$\Phi = 1, \quad \Gamma_\Phi = 0, \quad S_\Phi = 0 \qquad (2)$$

- momentum conservation

$$\Phi = u_i, \quad \Gamma_\Phi = \mu_{eff}, \quad S_\Phi = -\partial p / \partial x_i \qquad (3)$$

Turbulent Flow Modeling

Turbulent flow in the present study was simulated using four different models. They are the Baldwin-Lomax zero-equation model [1], the k-ε with wall function model [2], the k-ε Lam-Bremhorst model [3] and the k-ω two-equation model [4-5] were used for the analysis of DCA1 cascade.

Numerical Schemes

The governing equations were discretized in a non-staggered grid pattern and solved with a SIMPLE algorithm of Finite Volume Method. Hybrid scheme was used to discretize convection term. To prevent oscillatory pressure solutions due to the use of non-staggered grid, PWIM (Pressure-Weighted Interpolation Method) method of Rhie and Chow [6] were also used.

Specification of DCA1 and DCA2 (calculation conditions)

The specifications of cascade and flow conditions for respective cascade types, DCA1 and DCA2, were listed in Table. 1.

	DCA1	DCA2
Chord	228.6 mm	66.7 mm
Pitch	106.8 mm	46.7 mm
Height	368.1 mm	200 mm
AR	1.61	3
Solidity	2.14	1.43
Stagger angle	20.5°	51°
Camber angle	65.0°	13°
Incidence angle	-1.5°	-40°, 0°, 20°
Reynolds No.	5.0E5	0.72,1.2, 1.3E5

Table 1 Specification of cascades

Fig. 1 (a) and Fig.1 (b) show the configuration of cascade blades and the grid system used for DCA1 and DCA2 calculation, respectively.

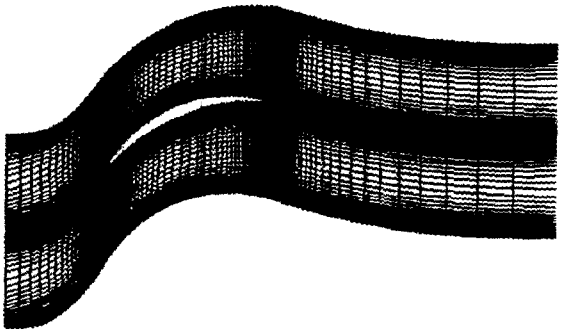

Fig. 1 (a) 2-D grid configuration for DCA1 [171×101]

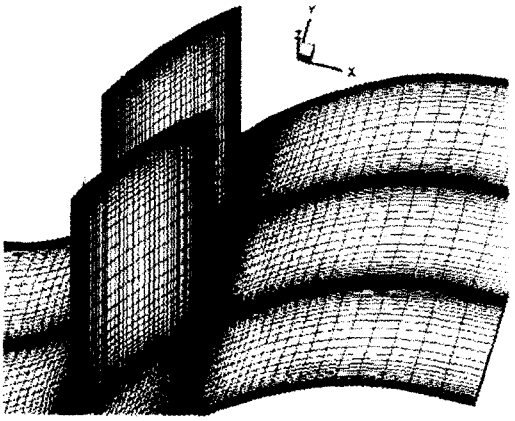

Fig. 1 (b) 3-D grid configuration for DCA2 [161 ×61×67]

Three dimensional grid system was established by the extension of two dimensional grid toward the third direction, z. Being careful to keep the orthogonality of grids near solid wall, H-type grids were collocated adjacent to the leading edge, trailing edge and cascade wall at which the significant changes of flow characteristics are expected.

Results

The computational results of DCA1 have been compared with those of Zierke et al. [7], while those of DCA2 compared with Hong et al. [8]

DCA1 for validation

Fig. 2 shows the distribution of static pressure coefficient on the cascade surface at -1.5° incidence. The pressure coefficient on blade surface is defined as;

$$C_p = \frac{P_2 - P_1}{\frac{1}{2}\rho V_1^2} \qquad (4)$$

where,

1 : flow inlet

2 : measurement position

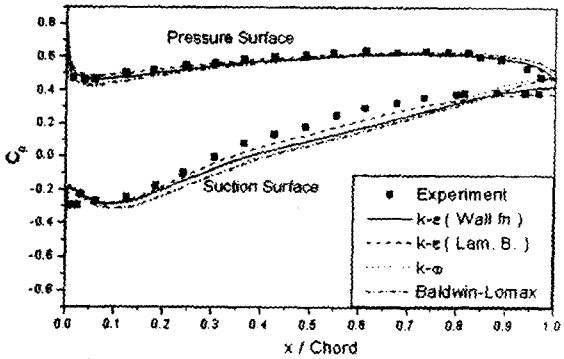

Fig.2 Distribution of pressure coefficient

The results of current study agree well with experimental results, but the pressure coefficient values show a little difference depending on turbulence model. At pressure surface, all the results show good agreement with experimental results except the results with Baldwin-Lomax model. Baldwin-Lomax model results show smaller pressure gradient near trailing edge than experimental data.

The suction surface is the region which has drastic flow changes. It could be found from Fig.2 that strong adverse pressure gradient region is observed at the leading edge and the favorable pressure gradient is formed between 4% chord to 10% chord downstream of the leading edge. The adverse pressure gradient region remains about 80% chord position and then turns into the favorable pressure gradient flow again. As Fig. 2 indicates that the result with k-ε Lam-Bremhorst model shows better agreement with experimental result than the others at suction surface.

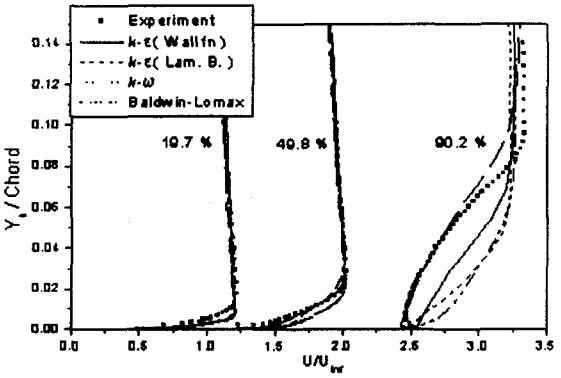

Fig.3 Velocity distribution on suction surface

Fig. 3 shows that the velocity distribution at 19.7%, 49.8% and 90.2% chord position on suction side, respectively. It could be found that the separated flow causes the discrepancies between current study and experiment at 90.2% chord position. Since no separations were observed at 19.7% and 49.8% chord position, current results are in a good agreement with the experiment. Among the results at 49.8% chord position, the k-ε with wall function model produced the most accurate velocity profiles. The k-ε Lam-Bremhorst model and the k-ω model predict the boundary layer thickness thinner than those of experiment. On the other hand, The Baldwin-Lomax model predicts the boundary layer thickness thicker than those of experimental result.

There is a recirculation region after the separation at 90.2% chord position; this could be an important factor for compressor cascade performance analysis. Table 2 shows the separation points each turbulence model predicted. Only the k-ε with wall function model couldn't predict the separation. But the results of k-ω model and Baldwin-Lomax model show considerable errors compared with experiment. In case of k-ε Lam-Bremhorst model, the prediction of separation point is agreed well with experimental result and also the size of recirculation is predicted similar to those of experiment. As a consequence, the velocity profile using k-ε Lam-Bremhorst model shows most exact result compared with experiment.

	Turbulence Model	Separation Point (% Chord)
Experiment		82.1
Numerical Result	k-ε with wall fn.	None
	k-ε Lam-Bremhorst	83.1
	k-ω	88.9
	Baldwin-Lomax	76.3

Table 2 Prediction of separation point

Compressor performance characteristics at the condition of high incidence angle (DCA2)

In this part, using another type of double-circular-arc cascade (DCA2), the two- and three-dimensional numerical analysis has been performed to predict the compressor performance characteristics at the condition of high incidence angle. Considering the result of previous chapter, the k-ε with wall function model was implemented in this part due to its advantage of grid savings, which is the popular two-equation turbulence model for general uses. The conservation equations and boundary conditions for turbulent kinetic energy and dissipation rate at solid wall are same as Launder and Spalding [2], while the boundary conditions for velocity and pressure are the conventional viscous flow conditions.

The profile of total pressure coefficient along pitch-direction at 50% chord length position by two- and three-dimensional calculation were compared with those of experiment in Fig 4 ~ Fig 6. The profile of total pressure coefficient at -10° incidence shows good agreement while the size of wake was under-estimated in calculation as shown in Fig. 4. And it is found that the total pressure coefficient values of three-dimensional profile are smaller than those of two-dimensional profile due to small momentum increases caused by the boundary layer from the third-directional walls.

Fig. 5 shows the pressure coefficient distribution at design incidence of 0°. The present and experimental results agree very well in the size of wake and the values of pressure coefficient. In this case, flow separation was not observed both in calculations and experiment.

At 12.5° incidence, as shown in Fig. 6, the significant loss increases in momentum and the discrepancies between calculations and experiment were found.

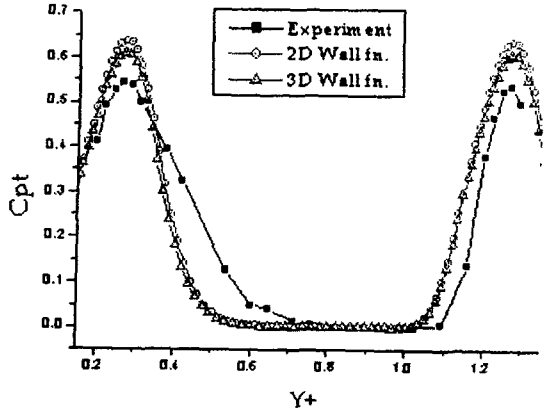

Fig.4 Total pressure loss coefficient profile at -10° incidence

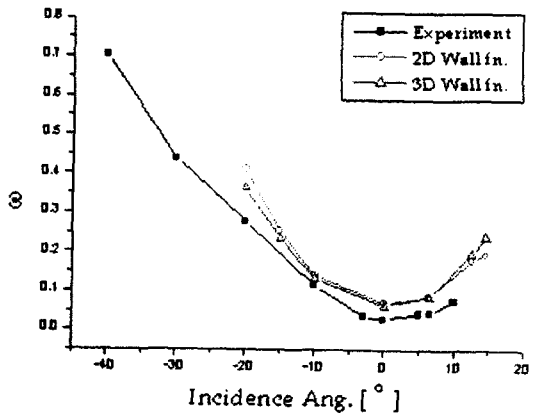

Fig.7 Mass averaged total pressure loss coefficient as incidence angle changes

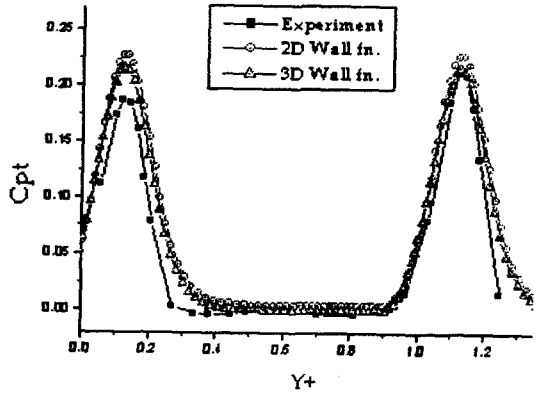

Fig.5 Total pressure loss coefficient profile at 0° incidence

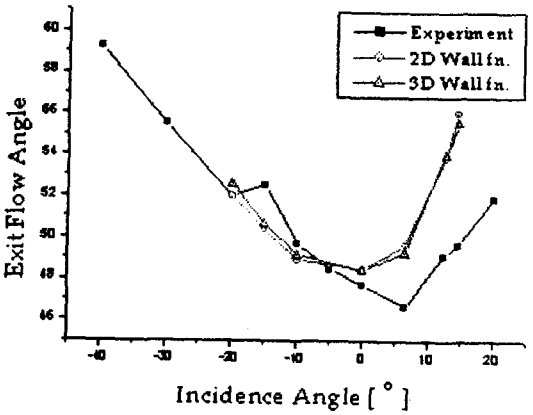

Fig.8 Exit flow angle as incidence changes

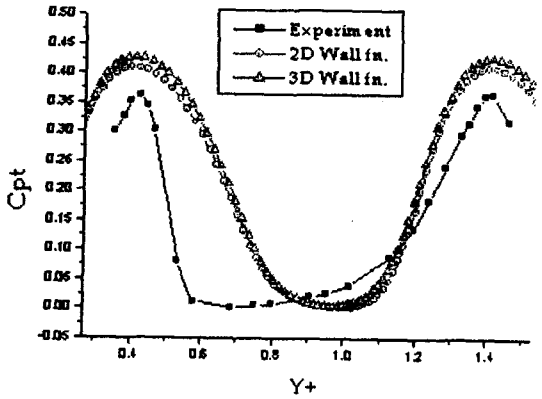

Fig.6 Total pressure loss coefficient profile at 12.5° incidence

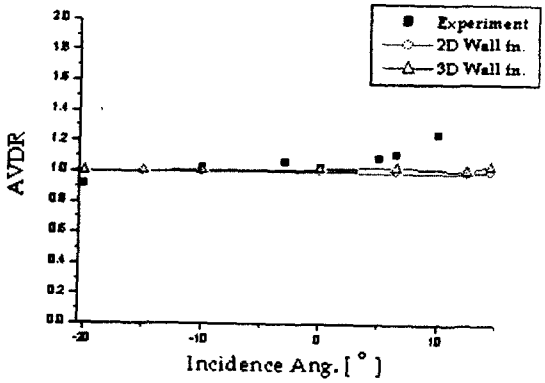

Fig.9 Axial velocity-density ratio as incidence changes

In this case, a considerable flow separation was observed due to high incidence.

The effect of incidence on the mass-averaged total pressure coefficients is shown in Fig. 7. The pressure coefficients have its minimum value at design incidence of 0° and increases as incidence increases.

The equation of mass-averaged total pressure coefficient is defined as

$$\omega = \frac{\int \rho V_x C_{pt} dy}{\int \rho V_x dy} \qquad (5)$$

Fig. 8 shows the exit flow angle for the whole incidence ranges and it could be found that the flow exit angle has its minimum values at design incidence of 0° and the deviation of values from the experiments increases as the incidence increases.

Fig. 9 represents the effect of incidence on the axial velocity-density ratio.

$$AVDR = \frac{\rho_2 V_{x2}}{\rho_1 V_{x1}} \qquad (6)$$

It was observed from Fig. 9 that the values of axial velocity-density ratio defined as equation (6) were almost 1.0 in both 2D and 3D calculations while those of experiment were larger than 1.0 because of the blockage effect as the incidence increases to the positive value. From this fact, it could be found that the decrease of flow area in calculations was predicted smaller than actual state though the separation was observed for 12.5° incidence.

The axial velocity profiles along span-wise direction on suction surface at 90% chord length position are shown in Fig. 10 for -10° incidence, Fig. 11 for 0° incidence and Fig 12 for 12.5° incidence, respectively. From these profiles shown in Fig 10, Fig. 11 and Fig. 12, it could be found that the velocity profiles are very similar with each other before separation and beyond boundary layer. In addition, separation causes the decrease of flow area which the main flow could pass through.

Along the span-wise direction, the contours of total pressure were extracted and shown in Fig. 13 for 0° incidence and Fig. 14 for 12.5° incidence. It was found that the total pressure loss would increase as the span-wise position approaches to upper and lower wall. Because the separation observed for 12.5° incidence was larger than that for 0° incidence, the total pressure loss would be increase as a result.

Conclusion

In this paper, the two- and three-dimensional numerical tool for cascade flow analysis were developed and used to investigate the flow characteristics through two types of double-circular-arc compressor cascades. The four different turbulence models were adopted to get more appropriate model for this subject. The numerical tool was verified for DCA1 cascade with the previous data by experiment and then could be used to investigate the cascade flow with confidence.

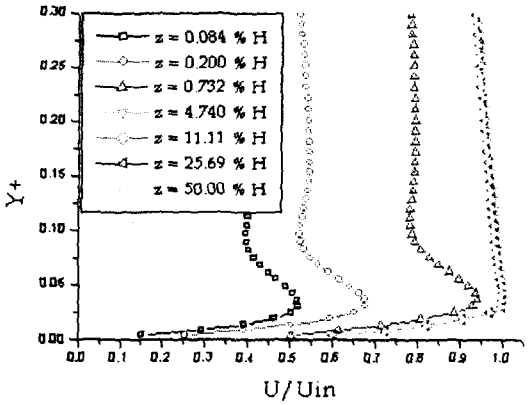

Fig.10 Axial velocity profile along the span at -10° incidence

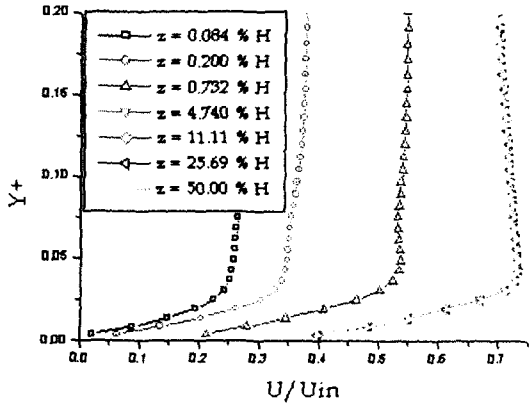

Fig.11 Axial velocity profile along the span at 0° incidence

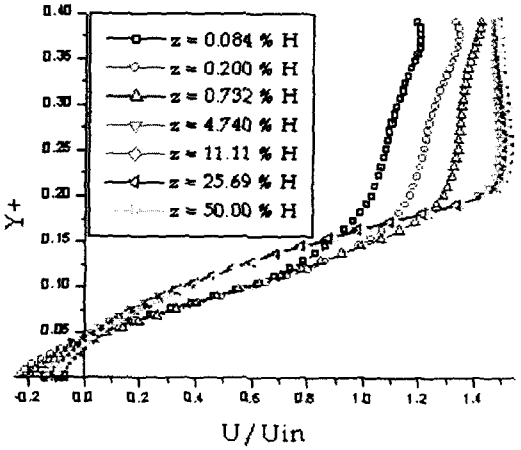

Fig.12 Axial velocity profile along the span at 12.5° incidence

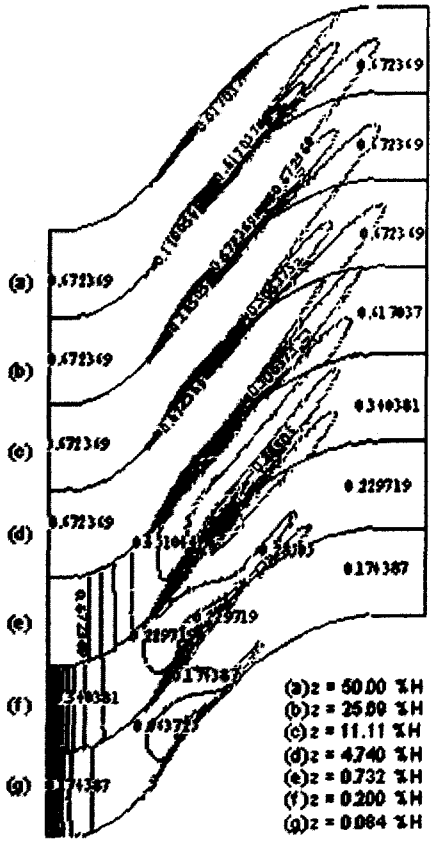

Fig.13 Total pressure along the span at 0° incidence

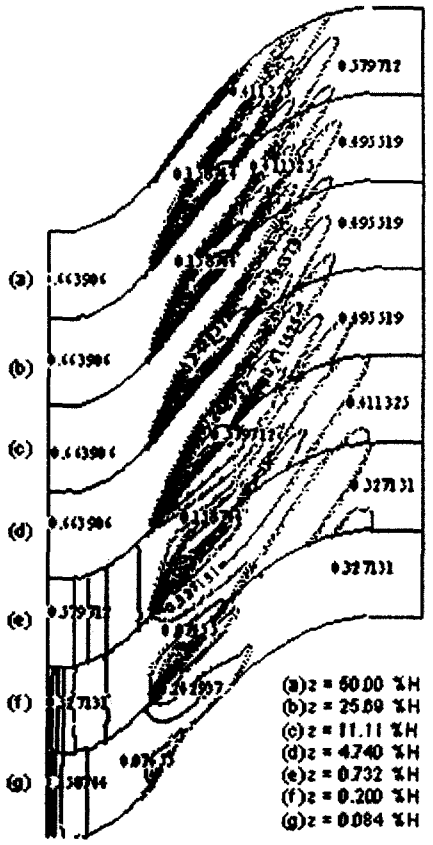

Fig.14 Total pressure along the span at 12.5° incidence

It was found that high incidence causes the flow through compressor cascade to be separated from the cascade surface and the acceleration effect caused by the cascade surface was not found which found for low incidence. Though the verification of our numerical tool was performed as mentioned above, the flow characteristics after separation could not be predicted well, which would be resolved in our next investigation.

References

1) Baldwin, B. S., and Lomax, H.: Thin Layer Approximation and Algebraic Model for Separated Flows, *AIAA Paper*, 1978, pp. 78-257.
2) Launder, B. E., and Spalding, D. B.: The Numerical Computation of Turbulent Flows, *Comp. Methods Appl. Mech. Eng.*, Vol. 3, 1974, pp. 269-289.
3) Lam , C. K. G., and Bremhorst, K.: A Modified Form of the k-ε Model for Predicting Wall Turbulence, *ASME Journal of Fluids Engineering*, Vol. 103, 1981, pp. 456-460.
4) Wilcox, D. C.: Reassessment of the Scale-Determining Equation for Advanced Turbulence Model, *AIAA Journal*, Vol. 26, No. 11, 1988, pp. 1299-1310.
5) Wilcox, D. C.: Simulation of Transition with a Two-Equation Turbulence Model, *AIAA Journal*, Vol. 32, No. 2, 1994, pp. 247-255.
6) Rhie, C. M., and Chow, W. L.: Numerical Study of the Turbulent Flow Past an Airfoil With Trailing Edge Separation, *AIAA Journal*, Vol. 21, 1983, pp. 1525-1532.
7) Zierke, W. C., and Deutsch, S.: The Measurement of Boundary Layers on a Compressor Blade in Cascade: Part 4-Flow Fields for Incidence Angles of -1.5 and -8.5 Degrees, *Journal of Turbomachinery*, Vol. 112, 1990, pp. 241-255.
8) Hong, G. R., Song, S. J., and Hong, Y. S.: The profile drag of axial compressor cascade at the various incidences, *Proc. of Korean society for aeronautical and space sciences*, Vol. 1, 1998, pp. 218-222.